Available online at www.sciencedirect.com
ScienceDirect
Journal of Molecular Catalysis A: Chemical 267 (2007) 224–233
JOURNAL OF MOLECULAR CATALYSIS A: CHEMICAL
www.elsevier.com/locate/molcata

The influence of preparation procedures and tungsten loading on the metathesis activity of ethene and 2-butene over supported WO_3 catalysts

Shengjun Huang, Fucun Chen, Shenglin Liu, Qingjun Zhu, Xiangxue Zhu, Wenjie Xin, Zaochi Feng, Can Li, Qingxia Wang, Longya Xu *

State Key Laboratory of Catalysis, Dalian Institute of Chemical Physics, Chinese Academy of Sciences, Dalian 116023, PR China

Received 18 October 2006; received in revised form 27 November 2006; accepted 28 November 2006
Available online 3 December 2006

Abstract

A series of catalysts composed of WO_3, γ-Al_2O_3 and HY were prepared to study the effects of preparation procedure and tungsten loading on their catalytic performances for the metathesis between ethene and 2-butene to propene. The catalysts are characterized by X-ray diffraction (XRD), temperature-programmed desorption of ammonia (NH_3-TPD), temperature-programmed reduction of hydrogen (H_2-TPR), N_2 adsorption, UV–vis and UV resonance Raman techniques. The results reveal that the catalytic activity is determined by the structure of supported tungsten oxide species. Based on the correlation between the activity and structure of tungsten oxide species, the isolated tetrahedral oxide species are suggested to be the active sites precursors, which exhibit characteristic Raman band at 970 cm^{-1}.

Keywords: Metathesis; WO_3–Al_2O_3–HY catalysts; Supported tungsten oxide species

1. Introduction

Since olefin metathesis was discovered serendipitously by Banks and Bailey 40 years ago, it has offered new industrial routes to important petrochemicals because it is a flexible process that can adapt the availability of alkenes according to the demand. The metathesis reaction of ethene and 2-butene is an alternative route to increase production of propene due to the strong global demand for this basic starting material of chemical industry. ABB Global has licensed this process as OCT (Olefin Conversion Technology), which uses WO_3/SiO_2 as the metathesis catalyst at >533 K and 30–35 bar [1]. It is reported the conversion of butene is above 60% per pass and the selectivity for propene is >90% [1]. However, the detailed description and characterization of the OCT practical catalysts are still scarce in the open literature. In contrast, more efforts have been devoted to the characterization and discussion of other supported WO_3 catalysts (WO_3/Al_2O_3 [2,3], WO_3/SiO_2 [4,5], WO_3/Al_2O_3–SiO_2 [6] and WO_3/TiO_2 [6]). One of the most interesting questions in the studies is nature of structure of active sites precursors. In general, WO_3 supported catalysts are composed of surface amorphous compound and crystalline trioxide depending on the surface concentration [7]. It has been confirmed extensively that WO_3 crystals are not active in metathesis and, as a consequence, the catalytic sites should be contained in the amorphous surface compound [4,7–9]. Thus far, the detailed study and discussion about the structure of amorphous surface compound are rare.

We reported recently that the WO_3 catalysts loaded on Al_2O_3–HY mixed support exhibited high activity for the metathesis between ethene and 2-butene, which achieved ~62% 2-butene conversion and 88% propene selectivity at 453 K and 0.1 MPa [10]. In the previous work, the activity of WO_3/Al_2O_3–HY catalysts was correlated with the Brönsted acidity and the interaction between tungsten species and support [10]. However, the structure of tungsten species upon this highly active catalyst has not been investigated. In the present study, a series of WO_3–Al_2O_3–HY catalysts are prepared and tested on the metathesis reaction between ethene and 2-butene. The catalytic activities are distinctively influenced by the preparation procedures and tungsten loadings. A variety of characterization

* Corresponding author. Tel.: +86 411 84693292; fax: +86 411 84693292.
E-mail address: lyxu@dicp.ac.cn (L. Xu).

1381-1169/$ – see front matter © 2007 Elsevier B.V. All rights reserved.
doi:10.1016/j.molcata.2006.11.048

results, especially the UV–vis and UV Raman spectra, reveal that isolated tetrahedral tungsten oxide species on these catalysts act as active sites precursors and are responsible for the metathesis activity.

2. Experimental

2.1. Support modification

γ-Al_2O_3 (FuShun Catalysts Manufactory, China) was calcined at 773 K for 2 h before use. HY zeolite (Wenzhou zeolite manufactory, $Si/Al_2 = 10$, $Na_2O < 0.2$ wt.%) was also calcined at 773 K for 2 h.

2.2. The preparation of catalysts

2.2.1. Catalysts prepared by different procedures

2.2.1.1. 10W/Al_2O_3–HY. Al_2O_3–HY mixed support was prepared by extrudating a mixture of 30 wt.% γ-Al_2O_3 powder and 70 wt.% HY zeolite. The drawn extrudate was dried at 393 K for 12 h and then calcined at 773 K for 2 h. The obtained sample was grinded into 16–32 mesh and was impregnated by ammonium metatungstate by incipient method, followed by calcination at 873 K for 2 h.

2.2.1.2. 10W/Al_2O_3/HY. This catalyst was prepared by firstly impregnating ammonium metatungstate on γ-Al_2O_3 by incipient method, followed by calcination at 873 K for 2 h. The calcined WO_3/Al_2O_3 was then physically mixed with HY zeolite and calcined at 873 K for 2 h.

2.2.1.3. 10W/HY/Al_2O_3. This catalyst was prepared by firstly loading the tungsten oxide on HY zeolite with ammonium metatungstate solution, followed by calcination at 873 K for 2 h. The calcined WO_3/HY was then physically mixed with γ-Al_2O_3, followed by calcination at 873 K for 2 h.

The compositions of catalysts above are the same, i.e.10 wt.% tungsten loading. Moreover, a mixture of bulk WO_3, γ-Al_2O_3 and HY was physically well mixed with the same weight ratio, and named as the reference sample of 10W–Al_2O_3–HY(mix). In addition, the comparative catalysts of 10W/Al_2O_3 and 10W/HY are prepared by impregnation method and calcined at 873 K for 2 h.

2.2.2. Catalysts with different tungsten loadings

A series of catalysts, prepared by the same procedures as 10W/Al_2O_3–HY catalyst, were denoted as yW/Al_2O_3–HY, where y represents the tungsten loading.

2.3. The evaluation of catalysts

The catalysts were tested in a fixed-bed flow microreactor of 10 mm inner diameter, and 3 g of catalyst with an average particle size of 0.56–1.3 mm was loaded. An EU-2 type thermocouple was fixed in the middle position of the catalyst bed at the outside of steel reactor to measure the temperature of electric furnace, which was taken as reaction temperature. After the catalyst was pretreated at 773 K for 1 h under high purity N_2 (0.1 MPa, 30 ml min^{-1}), it was cooled down to the reaction temperature. The reaction conditions are as follows: temperature = 453 K, pressure = 0.1 MPa, $N_2/C_2H_4 = 1.5$, C_2H_4/2-$C_4H_8 = 1$, WHSV = 1.5 h^{-1}. The metathesis activity was measured by 2-butene conversion, and the metathesis selectivity was estimated by the weight percent of propene in effluent gas [10].

2.4. Catalyst characterization

X-ray diffraction (XRD) measurements were performed with an XPert Pro PAnalytical Diffractometer using Cu Kα radiation, operating at 40 kV and 50 mA. Patterns were recorded from 3° to 70° (2θ).

Under flow of 10% H_2/Ar flow (20 ml min^{-1}), temperature-programmed reduction of hydrogen (H_2-TPR) profiles were obtained in the range of temperature from 473 to 1473 K at a programmed temperature rate of 14 K min^{-1} after the samples had been pretreated in Ar flow at 773 K for 30 min.

UV Vis spectra were recorded with a JASCO 500 spectrophotometer equipped with a diffuse reflectance attachment. The samples were studied in the form of 12-mm-diameter, 2-mm-thick pellets prepared as self-supporting wafers. The spectra were recorded under air-exposed conditions in the range 200–800 nm and the scan speed was 120 nm min^{-1}.

The UV Resonance Raman spectra were obtained on a homemade UV resonance Raman spectrograph. A 325.0 nm line from a He–Cd laser were used as the excitation source. The power of the laser lines were below 1.0 mW. Samples were mounted into a spinning holder to avoid thermal damage during the spectrum scanning which usually takes about 5 min. The spectra resolution was estimated to be 2.0 cm^{-1}.

Temperature-programmed desorption of ammonia (NH_3-TPD) measurements were performed in a conventional flow apparatus using a U-shaped microreactor (4 mm, i.d.) made of stainless steel, with helium (He) as the carrier gas. The NH_3-TPD process was monitored by a gas chromatograph with a TCD detector. A catalyst sample of 0.14 g was pretreated at 873 K for 0.5 h in a He stream with a flow rate of 25 ml min^{-1} and was cooled to 423 K. Then, it was exposed to an NH_3-containing He stream for 10 min. The sample was purged with a pure He stream for a certain period of time until a constant baseline was attained. NH_3-TPD was carried out in the range of 423–873 K at a heating rate of 18 K min^{-1}.

Nitrogen adsorption measurements were carried out at 77 K on an ASAP 2010 automatic adsorption analyzer equipped with the micropore options (from Micromeritics). Before the measurements, samples of ca. 0.1 g were placed in the degas port of the adsorption apparatus, degassed at 383 K for 1 h and at 623 K for 4 h. The data from the low-pressure region were obtained by contacting the sample with successive increases of analysis gas until the thermal equilibration was reached. Adsorption isotherms were measured under the relative pressure range, based on the saturation vapor pressure which is from $\sim 10^{-7}$ to 0.1 MPa.

Table 1
Surface area (SA) ($m^2\ g^{-1}$) and pore volume (PV) ($cm^3\ g^{-1}$) of WO_3 catalysts prepared by different procedures

	Samples			
	Reference sample: 10W–Al_2O_3–HY(mix)	10W/Al_2O_3–HY	10W/Al_2O_3/HY	10W/HY/Al_2O_3
SA (BET)	486	370	429	362
Micro-pore-volume (H–K)	0.206	0.155	0.182	0.153
Meso-pore-volume (BJH)	0.237	0.190	0.153	0.202

3. Results

3.1. The characterization results of catalysts prepared by different procedures

The specific surface area, micropore and mesopore volume of the catalysts are listed in Table 1. 10W/Al_2O_3–HY and 10W/HY/Al_2O_3 catalysts possess the smaller BET surface area of 370 and 362 $m^2\ g^{-1}$, whereas 10W/Al_2O_3/HY shows the larger value of 429 $m^2\ g^{-1}$. The value of micropore volume follows the similar sequence. 10W/Al_2O_3/HY catalyst possesses the larger volume of 0.182 $cm^3\ g^{-1}$ while 10W/Al_2O_3–HY and 10W/HY/Al_2O_3 exhibit smaller values of 0.155 and 0.153 $cm^3\ g^{-1}$, respectively. On the contrary, 10W/HY/Al_2O_3 has the largest mesopore volume compared with 10W/Al_2O_3–HY and 10W/Al_2O_3/HY. In contrast to the reference sample of 10W–Al_2O_3–HY(mix), all of catalysts prepared by the impregnation method show decreased surface area, micropores and mesopores volume, indicating the modification of tungsten species on the micro-structure of HY and Al_2O_3 components. Such modification on 10W/Al_2O_3–HY and 10W/Al_2O_3/HY is more pronounced than that of 10W/HY/Al_2O_3, which may be resulted from the different nature of tungsten oxide species due to different preparation procedures.

XRD patterns of WO_3 catalysts prepared by different procedures are given in Fig. 1. All samples do not show characteristic diffraction peaks of γ-Al_2O_3, which is due to the low sensitivity of γ-Al_2O_3 to X-ray. The patterns of 10W/Al_2O_3–HY and 10W/Al_2O_3/HY catalysts also do not exhibit any diffraction peaks of WO_3 crystal, indicating tungsten species form the amorphous surface compound or microcrystallites that can not be detected at this measuring scale. In contrast, 10W/HY/Al_2O_3 catalyst shows minor characteristic diffraction peaks of WO_3 crystal (2θ: 23.12 and 23.60°), indicating part of tungsten species over 10W/HY/Al_2O_3 catalyst form WO_3 microcrystallites or WO_3-like phase.

The interaction between tungsten oxide species and supports (metal–support interaction) was characterized by H_2-TPR technique. As shown in Fig. 2, the profile of reference sample 10W–Al_2O_3–HY(mix) reveals a complete reduction of bulk WO_3 to W metal, which is different from those of supported WO_3 catalysts. The profile of 10W/Al_2O_3–HY catalyst exhibits two small and broad reduction peaks at around 993 and 1183 K. The reduction peak at lower temperature has been attributed to the reduction of octahedral tungsten oxide species [11], and the reduction peak at higher temperature has been assigned to the reduction of well-dispersed W species rich in tetrahedral coordination [12]. The smallest reduction peaks belong to 10W/Al_2O_3/HY, which is just more intensive than those of previous 10W/Al_2O_3 sample [10]. The reduction profile of 10W/Al_2O_3/HY exhibits two minor reduction peaks at 993 and 1163 K, which can be attributed to reduction of octahedral and tetrahedral tungsten oxide species [11,12], respectively. As a comparison, 10W/HY/Al_2O_3 catalyst shows a broad reduction peak at 1113 K, which can be attributed to the reduction of polytungstate species and WO_3 crystallites [13,14]. This is corroborated by the XRD pattern that significant amount of crystal WO_3 is present

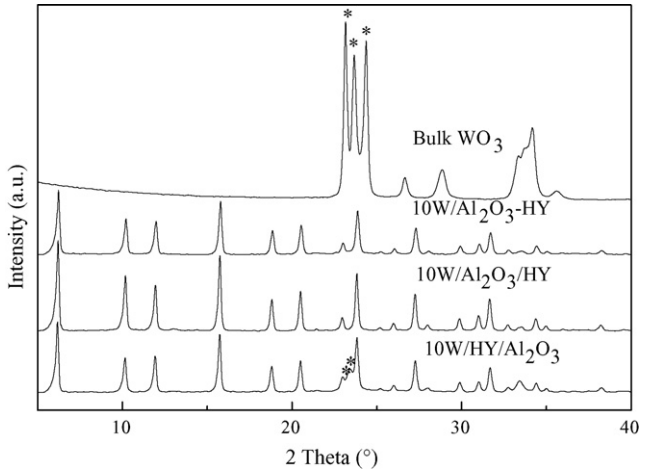

Fig. 1. The XRD patterns of WO_3 catalysts prepared by different procedures.

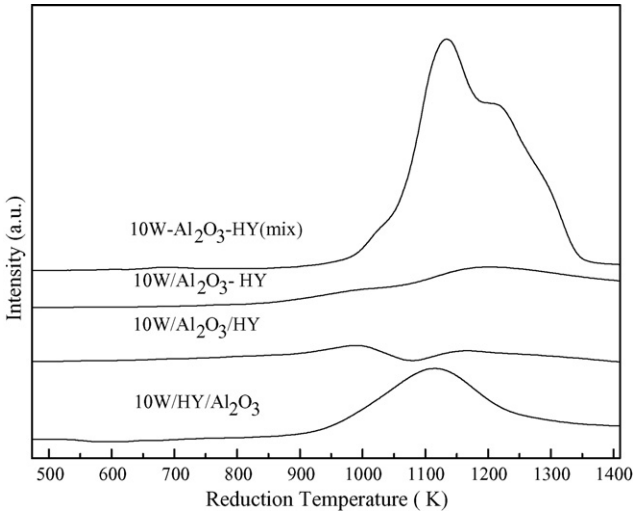

Fig. 2. The H_2-TPR profiles of WO_3 catalysts prepared by different procedures.

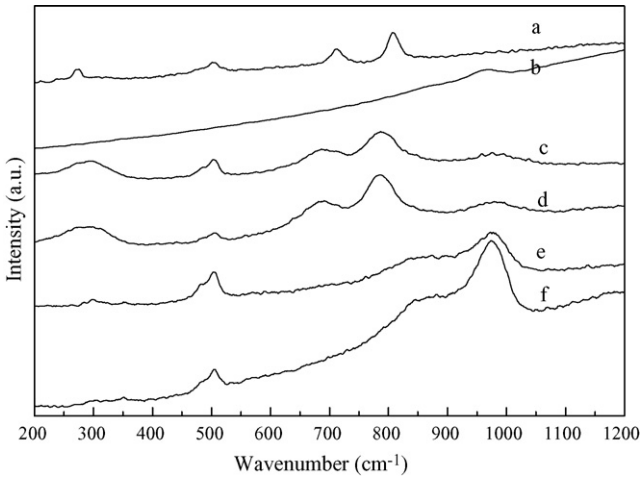

Fig. 3. The UV resonance Raman spectra of WO_3 catalysts prepared by different procedures. (a) 10W–Al_2O_3-HY(mix); (b) 10W/Al_2O_3; (c) 10W/HY; (d) 10W/HY/Al_2O_3; (e) 10W/Al_2O_3/HY; (f) 10W/Al_2O_3–HY.

on 10W/HY/Al_2O_3. These profiles are remarkably different from each other, and the area of reduction peaks decrease as 10W/HY/Al_2O_3 > 10W/Al_2O_3–HY > 10W/Al_2O_3/HY. Since the tungsten loadings are the same, the results suggest that different preparation procedures lead to different metal–support interactions. It is proposed that 10W/Al_2O_3/HY and 10W/Al_2O_3–HY possess relative stronger metal–support interaction than 10W/HY/Al_2O_3.

The UV Resonance Raman spectra provide further information on the structural characteristics of supported tungsten species, and the spectra of various samples are presented in Fig. 3. According to the literature, the Raman band around 500 cm^{-1} are mainly due to O–Si–O bending character of faujasite zeolite [15], which is present in all samples except for 10W/Al_2O_3. On the other hand, the fluorescence phenomena are observed for all catalysts except 10W/HY, due to the fluorescence effect of alumina component [16]. The reference sample of 10W–Al_2O_3–HY(mix) exhibits the bands at about 805, 706 and 273 cm^{-1} [12,17,18], where 805 and 706 cm^{-1} are assigned to stretching vibration of W–O–W and 273 cm^{-1} to W–O–W bending mode. The absence of bands at 1046–1057, 386 and 371 cm^{-1} excludes the formation of $Al_2(WO_4)_3$ for all catalysts. As shown in Fig. 3, 10W/HY and 10W/HY/Al_2O_3 exhibit similar spectra, both present broad bands at 290, 690 and 790 cm^{-1} with a minor band at 970 cm^{-1}. It is proposed that 805, 706 and 273 cm^{-1} bands due to bulk WO_3 are overlapped by those three broad bands. However, they cannot be assigned to any well-defined structure according to present available literatures. Nevertheless, their position is rather close to that of WO_3 crystal, and we suggest they are caused by some WO_3-like polytungstate. It is found that the spectra of 10W/Al_2O_3–HY and 10W/Al_2O_3/HY are similar, exhibiting relative intensive bands at 840–880 cm^{-1} and 970 cm^{-1}. According to the literature [12,19], the 840–880 cm^{-1} band is assigned to asymmetric stretch mode of a W-O-W linkage, corresponding to two-dimensional surface polytungsten oxide species. However, the precise assignment of 970 cm^{-1} band is ambiguous. Horsley et al have concluded that there is much overlap in the band positions of the octahedral and tetrahedral tungsten species in the regions of 910–970 cm^{-1}, which should be carefully utilized to adequately differentiate these two species [18]. The spectra of 10W/Al_2O_3 give additional information for the discrimination. Since the 10 wt.% tungsten loading is about 1/3 of monolayer coverage on WO_3/Al_2O_3, and it is found with in situ XANES that tungsten species is predominantly present as a distorted tetrahedral species at this coverage [18]. Therefore, the Raman bands at about 880 and 956 cm^{-1} could be assigned to the asymmetric stretch of W=O of isolated tetrahedral tungsten species and symmetric stretch of W=O in distorted tetrahedral tungsten species, respectively [18,20].

The ~956 cm^{-1} Raman band shifts to higher wavenumbers with the weakened metal–support interaction. For WO_3/Al_2O_3-TiO_2 catalysts, the Raman band, due to symmetric stretching vibration mode of W=O bonds in tetrahedral tungsten species, shifts from 957 cm^{-1} to ~977 cm^{-1} when the titanium content is increased. This observed phenomenon has been attributed to the increase of lateral interaction, which is partly resulted from the decreased metal-support interaction of tungsten species with the Al_2O_3–TiO_2 support [12]. Moreover, it was reported that the band at ~950 cm^{-1} shifts to ~970 cm^{-1} with the increasing tungsten loading [20]. As suggested by H_2-TPR results, the addition of HY zeolite as support results in more population of reducible tungsten oxide species than 10W/Al_2O_3, indicating the decreased metal-support interaction and the increased lateral interaction between metal oxide species. Hence, the 956 cm^{-1} band of 10W/Al_2O_3 shifts to higher wavenumbers of 970 cm^{-1} for 10W/Al_2O_3–HY and 10W/Al_2O_3/HY, and it is assigned to the vibration mode of W=O bonds in isolated surface tetrahedral tungsten oxide species.

The NH_3-TPD curves display the effect of preparation procedures on the acidity of the catalysts in Fig. 4. Our previous results indicate that γ-Al_2O_3 exhibits a broad band centered at about 533 K, which is generally assigned to weak acid sites (not shown). For HY zeolite, in addition to the weak acid sites, another higher-temperature desorption peak is observed

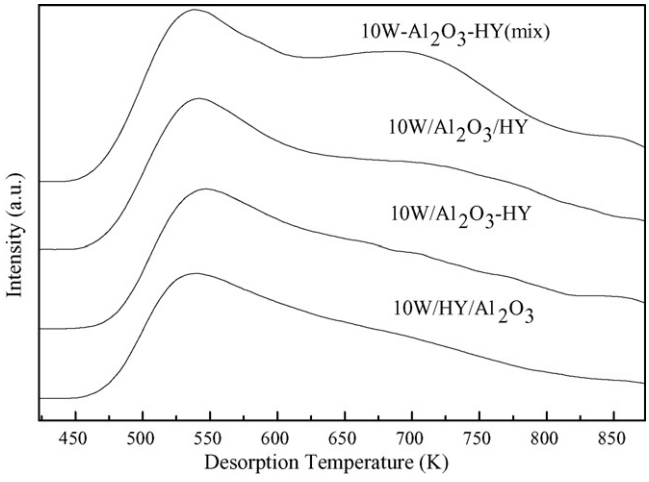

Fig. 4. The NH_3-TPD profiles of WO_3 catalysts prepared by different procedures.

in the temperature range of 633–813 K, suggesting presence of stronger acid sites on HY zeolite. As shown in Fig. 4, the reference sample of 10W–Al_2O_3–HY(mix) shows a sharp peak at about 533 K and another two broad peaks in the temperature range of 633–813 K, respectively. For all catalysts, the intensities of these three peaks decrease, particularly for the desorption peaks in the higher temperature range. However, it is difficult to precisely clarify the interconversion of Brönsted and Lewis acid sites after the incorporation of tungsten species, particularly with the fact that both HY zeolite and Al_2O_3 were employed as support. According to the literature [21], the addition of WO_3 to γ-Al_2O_3 has been proved to increase the Brönsted acidity at the expense of Lewis acidity, and maintain acid density constant simultaneously. Consequently, the reduction of strong acid sites should be mostly attributed to the consumption of Brönsted acid sites of HY zeolite by the surface tungsten oxide species during the impregnation and calcination process [22,23]. The total amount of acid sites are directly compared by the integrated areas of each NH_3-TPD curves, which follows the sequence of 10W/Al_2O_3/HY > 10W/Al_2O_3–HY > 10W/HY/Al_2O_3. This also implicates the amount of tungsten species interacted with Brönsted acid sites. Clearly, the impregnation of tungsten precursor with HY support first in the preparation, i.e. 10W/HY/Al_2O_3, results in the most pronounced interaction of Brönsted acid sites with the tungsten species.

3.2. The characterization results of WO_3/Al_2O_3–HY catalysts with different tungsten loadings

The XRD patterns of WO_3/Al_2O_3–HY catalysts with different tungsten loading are shown in Fig. 5. When the tungsten loadings are lower than 18 wt.%, the patterns do not show diffraction peaks of WO_3, indicating a well dispersion of tungsten species to form the amorphous surface compound or microcrystallites which are invisible by XRD at this measure scale. After the tungsten loading is increased to 18 wt.%, a slight diffraction peak of WO_3 microcrystallites is observed (2θ: 23.60°), and the intensity of HY zeolite characteristic peaks decreases simultaneously. This minor diffraction peak turns into the characteristic peaks of WO_3 crystal (2θ: 23.12, 23.60 and 24.38°) when the tungsten loading reaches 24 wt.%, for which the structure of HY zeolite is obviously destroyed. The decreased crystallinity of HY zeolite is due to the deformation effect of tungsten species on the zeolite framework [22,23]. The transformation of XRD patterns indicates the state of tungsten species on the Al_2O_3–HY support could turn from amorphous surface compound to WO_3 crystal with the increase of the tungsten loading.

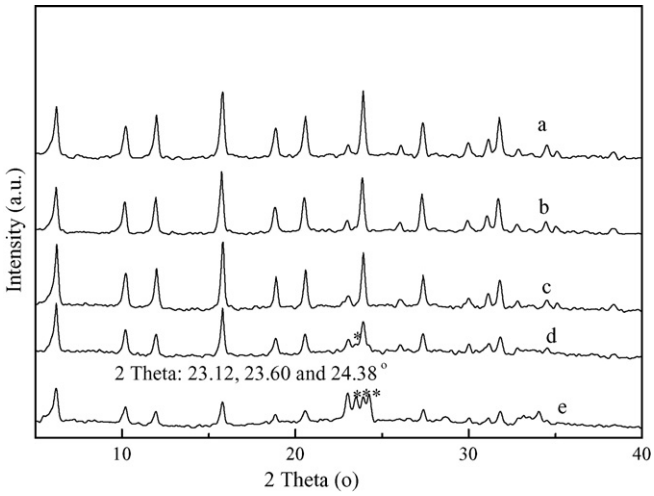

Fig. 5. The XRD patterns of WO_3/Al_2O_3–HY catalysts with different W loading. (a) 4W/Al_2O_3–HY; (b) 7W/Al_2O_3–HY; (c) 13W/Al_2O_3–HY; (d) 18W/Al_2O_3–HY; (e) 24W/Al_2O_3-HY. (*) The diffraction peaks of WO_3.

The effect of tungsten loadings on the coordination state of tungsten species is also investigated by UV Vis spectra as shown in Fig. 6. The measured spectra are deconvoluted into the lowest possible number of Gaussian subbands, and the relative intensities of those subbands are listed in Table 2. The reference sample of 10W–Al_2O_3–HY(mix) (Fig. 6-a) is dominated by characteristic broad bands in the region of 230–400 nm, which consists of three subbands at 280, 340 and 380 nm. These subbands are attributed to charge transfer (CT) of W^{6+} species in normal and distorted octahedral coordination [12,24–26], since bulk WO_3 is completely in the octahedral symmetry. The spectra of supported WO_3 catalysts are remarkably different from that of bulk WO_3. Their spectra are deconvoluted into three subbands at 220, 260 and 340 nm in the loading range of 4–18 wt.%. The subbands can be assigned as follows: 210–220 nm band to tetrahedral tungsten oxide species; 250–280 nm one to octahedral polytungstate species and 340 nm band to octahedral species in WO_3 or WO_3-like polystructure [12,24–26]. As shown in Table 2, the absolute intensity of 220 nm subbands increases with the increase of tungsten loading and achieves the maximum at

Table 2
The absolute intensities of subbands derived from deconvolution of UV–vis spectra of WO_3/Al_2O_3–HY catalysts with different tungsten loading and their contributions to each complete spectrum

Catalyst	I_{220}[a]	I_{260}[a]	I_{280}[a]	I_{340}[a]	I_{380}[a]
4W/Al_2O_3–HY	38 (51%)	35 (47%)	–	1.6 (2%)	–
7W/Al_2O_3–HY	49 (50%)	46 (47%)	–	3 (3%)	–
10W/Al_2O_3–HY	63 (42%)	81(54%)	–	5.3 (4%)	–
13W/Al_2O_3–HY	73 (41%)	96 (54%)	–	9.4 (5%)	–
18W/Al_2O_3–HY	66 (34%)	111 (58%)	–	14.2 (8%)	–
24W/Al_2O_3–HY	58 (27%)	111 (52%)		[22, 19, 3.6][b] (21%)	

[a] The list value outside is the absolute intensity of subbands and the value inside is the relative percent to the intensity of whole band.
[b] The value in the square bracket is the intensities of subbands to WO_3 crystal.

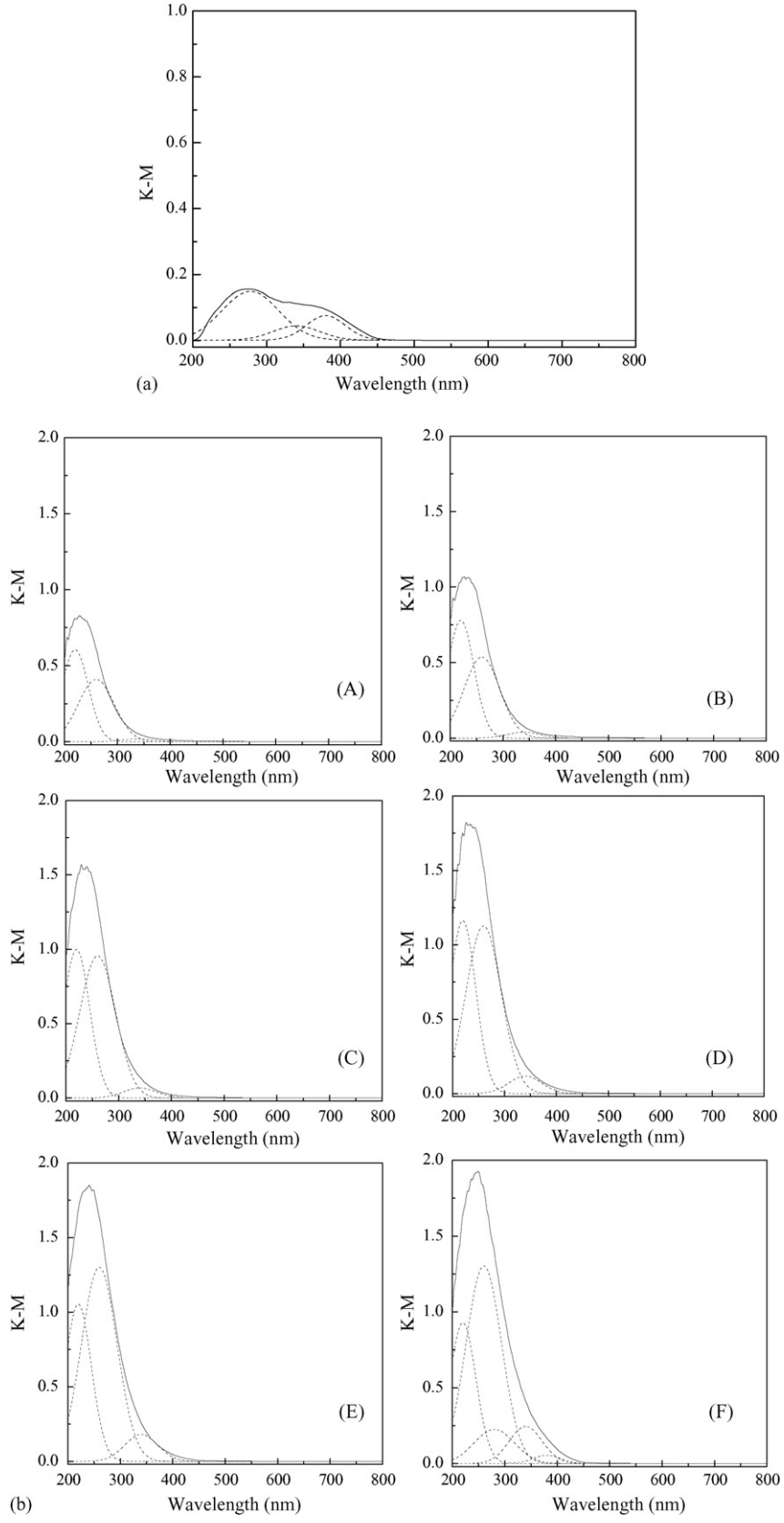

Fig. 6. The UV–vis spectra of WO_3/Al_2O_3–HY with different tungsten loading. (a) 10W-Al_2O_3–HY(mix); (b)—A, 4W/Al_2O_3–HY; B, 7W/Al_2O_3–HY; C, 10W/Al_2O_3–HY; D, 13W/Al_2O_3–HY; E, 18W/Al_2O_3–HY; F, 24W/Al_2O_3–HY.

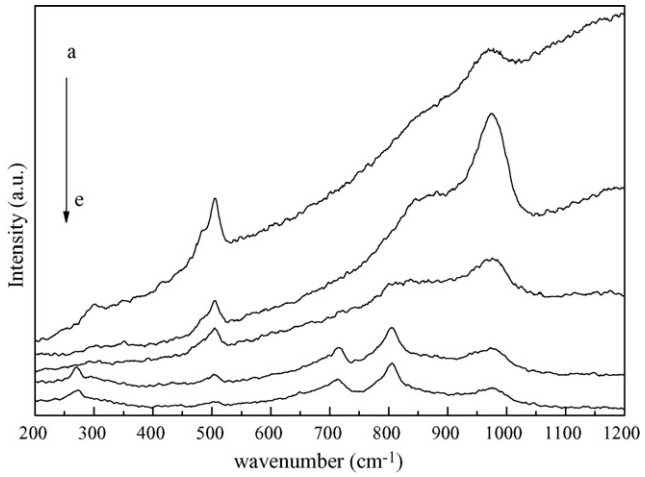

Fig. 7. The UV resonance Raman spectra of WO_3/Al_2O_3–HY catalysts with different tungsten loading. (a) $4W/Al_2O_3$–HY; (b) $10W/Al_2O_3$–HY; (c) $13W/Al_2O_3$–HY; (d) $18W/Al_2O_3$–HY; (e) $24W/Al_2O_3$–HY.

the 13 wt.% loading, pointing to the increase of tetrahedral tungsten species in the tungsten loading range of 4–13 wt.%. Further increase (>13 wt.%) of loading causes this subband to decrease, indicating the transformation of these tetrahedral species. As a comparison, the absolute intensities of 260 and 340 nm subbands increase consistently with the increased tungsten loading, indicating a sustained increase of octahedral tungsten species. However, the spectrum of $24W/Al_2O_3$–HY is distinctly different, which is deconvoluted into five subbands at 220, 260, 280, 340 and 380 nm. The latter three subbands agree with the deconvolution of bulk WO_3, suggesting the formation of WO_3 crystal from surface tungsten oxide species. Furthermore, the ratio of octahedrally coordinated tungsten species to tetrahedrally coordinated tungsten ones increases with the increased tungsten loading. Finally, WO_3-like polystructure and WO_3 crystal are formed. This is in agreement with the transformation of tungsten oxide species on WO_3/γ-Al_2O_3 as the function of loadings [27].

UV resonance Raman spectra offer additional information for the structure of tungsten species with the increase of tungsten loadings. As shown in Fig. 7, the fluorescence effect due to γ-Al_2O_3 diminishes with the increase of tungsten loading. It is evident that the fluorescence effect disappears with tungsten loading higher than 18 wt.%, indicating a full coverage of γ-Al_2O_3 surface by tungsten species. Simultaneously, the band at about 500 cm^{-1}, characteristic of the Si–O–Si bending mode of faujasite zeolite, also diminishes with the increase of tungsten loading, indicating a deterioration effect of tungsten species on the framework of HY zeolite. Moreover, the band at 500 cm^{-1} almost vanishes for the $24W/Al_2O_3$–HY catalyst, suggesting a remarkable loss of crystallinity which is underpinned by XRD patterns.

When the tungsten loading is below 10 wt.%, the bands at 970 cm^{-1} and 840–880 cm^{-1} become more pronounced with the increase of tungsten loadings. However, the spectra show more complex features with higher tungsten loading. For $13W/Al_2O_3$–HY catalyst, a new band appears at about 803 cm^{-1}, which has been assigned to the highly dispersed WO_3 microcrystallites [12,16,17], whereas the bands at 970 cm^{-1} and 840–880 cm^{-1} decrease. As the tungsten loading reaches 18 wt.%, the band in 840–880 cm^{-1} region is not observed, accompanied by a continuously decreased 970 cm^{-1} band. New bands at 273, 706, and 805 cm^{-1} also appear, indicating the existence of grown WO_3 crystal. The spectrum of $24W/Al_2O_3$–HY is similar to that of $18W/Al_2O_3$–HY. However, it exhibits the slightest 970 cm^{-1} band despite of its highest tungsten loading.

From the intensities of Raman bands, we can compare the amount of different tungsten species. In the range of 4–10 wt.%, the intensified 970 cm^{-1} bands indicate the increasing amount of isolated tetrahedral tungsten oxide species. This band becomes diminished with higher tungsten loadings, especially for $18W/Al_2O_3$–HY and $24W/Al_2O_3$–HY. Nevertheless, crystalline WO_3 possesses a Raman scattering cross-section that is much greater than the surface tungsten oxide surface species by ~160× [28]. Due to the relative stronger signals of WO_3 crystallites, the estimation of amount of surface tungsten oxide species can be misleading just by the intensity of Raman bands with tungsten loading higher than 13 wt.%. However, a rough estimation still can be done with the assistance of UV–vis spectra. UV–vis spectra (Fig. 6) and Table 2 reveal that the amount of tetrahedral tungsten species is abundant on $18W/Al_2O_3$–HY after the maximum on $13W/Al_2O_3$–HY. Taking into account the comparable intensities of 970 cm^{-1} bands in their UV Raman measurement, the amount of isolated tetrahedral tungsten oxide species on $13W/Al_2O_3$–HY and $18W/Al_2O_3$–HY are rather rich and comparable to that of $10W/Al_2O_3$–HY. The slightest 970 cm^{-1} Raman band plus the significantly decreased 220 nm subband (Table 2) confirm the remarkable decrease of isolated tetrahedral tungsten oxide species on $24W/Al_2O_3$–HY. The two-dimensional surface polytungsten species also increase with the enhancement of 840–880 cm^{-1} Raman band from 4 to 10 wt.%. However, these species decrease on $13W/Al_2O_3$–HY, evidenced by the distinctively diminished 840–880 cm^{-1} Raman band. In fact, two-dimensional surface polytungsten species vanish on $18W/Al_2O_3$–HY and $24W/Al_2O_3$–HY as evidenced by the indistinguishable 840–880 cm^{-1} band. The disappearance of these two-dimensional surface polytungstate species may also contribute to the transformation of surface tungsten species to WO_3-like polystructure and WO_3 crystallites during calcination process, which is corroborated by the appearance of characteristic Raman band of WO_3 crystallites.

3.3. The effect of preparation procedures and tungsten loading on the catalytic activity of WO_3 catalysts

The influence of preparation procedures on the metathesis between ethene and 2-butene is investigated at 453 K. The 2-butene conversion and weight percent of propene in effluent gas were used to evaluate the activity and selectivity. The bulk WO_3 does not show any metathesis activity, which agrees with the report that the unsupported bulk WO_3 is not active for olefin metathesis [29]. After the tungsten oxide was loaded on the support, the catalysts show catalytic activities for the metathesis reaction. However, the metathesis activities are

Table 3
The catalytic performance of tungsten-based catalysts prepared by different procedures

Catalyst	2-$C_4^=$ conversion (%)	Selectivity (%)		
		$C_3^=$	1-$C_4^=$[a]	C_5 andC_5^+[b]
10W/Al_2O_3–HY	62.8	88.1	6.3	5.6
10W/Al_2O_3/HY	47.6	81.3	9.4	9.3
10W/HY/Al_2O_3	27.1	58.1	27.5	14.4
10W/Al_2O_3	23.6	64.0	22.6	13.4
10W/HY	16.6	36.2	46.7	17.1

Reaction condition: $T = 453$ K; $P = 0.1$ MPa; WHSV = 1.5 h^{-1}; ethene/2-butene = 1 (mole ratio); TOS = 0.5 h.
[a] 1-$C_4^=$: the side products of 1-butene and isobutene.
[b] C_5 and C_5^+: the side products possessing five or higher carbon numbers.

remarkably influenced by the preparation procedures as shown in Table 3. 10W/Al_2O_3–HY catalyst exhibits superior catalytic performance, i.e. 62.8% 2-butene conversion and 88.1% propene selectivity. However, if the tungsten oxide were firstly loaded on Al_2O_3 then mixed with HY zeolite, the catalyst 10W/Al_2O_3/HY shows decreased metathesis activity, i.e., 47.6% 2-butene conversion and slightly decreased propene selectivity of 81.3%, It is worth noting that they are still superior to 23.6% 2-butene conversion and 64.0% propene selectivity of 10W/Al_2O_3. The poorest results occur on the 10W/HY/Al_2O_3, showing only 27.1% 2-butene conversion and 58.1% propene selectivity, but are much better than 16.6% 2-butene conversion and 36.2% propene selectivity of 10W/HY.

The effect of tungsten loadings on the metathesis activity of WO_3/Al_2O_3–HY catalyst is also investigated. As shown in Fig. 8, 2-butene conversion increases from 32.8 to 62.8% with the increase of tungsten loading from 4 to 10 wt.%. Then, the 2-butene conversion reaches a plateau of ~62% with the tungsten loading in the 10–18 wt.% range. Nevertheless, 2-butene conversion undergoes a remarkable decrease to 45.5% for 24W/Al_2O_3–HY. The metathesis activity as the function of tungsten loading is an inversed "U" type. The propene selectivity as the function of tungsten loading follows the same

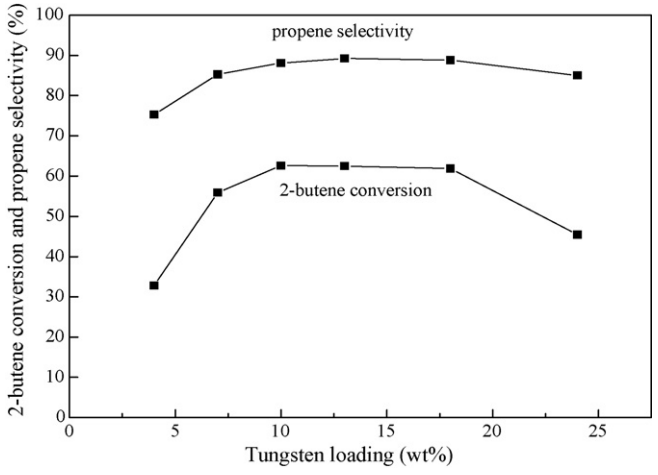

Fig. 8. The dependence of metathesis activity on the tungsten loading for the WO_3/Al_2O_3–HY catalysts. Reaction condition: $T = 453$ K; $P = 0.1$ MPa; WHSV = 1.5 h^{-1}; ethene/2-butene = 1 (mole ratio); TOS = 1.0 h.

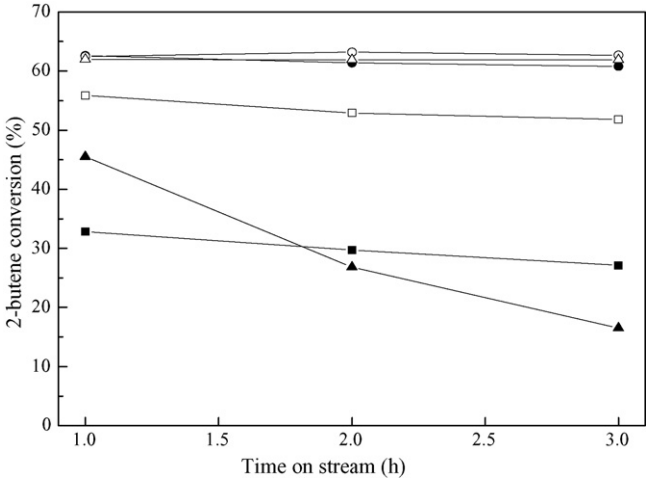

Fig. 9. The activity of WO_3/Al_2O_3–HY catalysts with different tungsten loading as the function of reaction time. Reaction condition: $T = 453$ K; $P = 0.1$ MPa; WHSV = 1.5 h^{-1}; ethene/2-butene = 1 (mole ratio). (■) 4W/Al_2O_3–HY; (□) 7W/Al_2O_3–HY; (●) 10W/Al_2O_3–HY; (○) 13W/Al_2O_3–HY; (△) 18W/Al_2O_3–HY; (▲) 24W/Al_2O_3–HY.

trend. The variation of metathesis activity of different catalysts as a function of reaction time is shown in Fig. 9. It can be seen that 4W/Al_2O_3–HY and 7W/Al_2O_3–HY show a slightly decreased 2-butene conversion from 32.8 to 27.1% and 55.9 to 51.8%, respectively. The active catalysts, i.e. 10W/Al_2O_3–HY, 13W/Al_2O_3–HY and 18W/Al_2O_3–HY possess relatively stable 2-butene conversion at about 60% within 3 h reaction time. In contrast, 2-butene conversion on 24W/Al_2O_3–HY undergoes a sharp decrease from 45.5 to 16.5% in 3 h, indicating a quick deactivation of this catalyst.

4. Discussion

Compared with the 10W/Al_2O_3 and 10W/HY, the combination of Al_2O_3 and HY zeolite as supports definitely improves the metathesis activity of 10W/Al_2O_3–HY, 10W/Al_2O_3/HY and 10W/HY/Al_2O_3 catalysts. However, the extent of promoting effect remarkably depends on the preparation procedures. It has been proposed that the Brönsted acid sites can directly favor the formation of active sites [30], or interact with the metal species, leading to the precursors of most active sites [31]. However, despite of the largest amount of Brönsted acid sites of 10W/Al_2O_3/HY in our NH_3-TPD results, the catalyst does not exhibit the most significant promoting effect. On the other hand, although 10W/HY/Al_2O_3 has the largest amount of tungsten species that interact with Brönsted acid sites, the catalytic performance is still relatively poor. Indeed, the metathesis activities follow the sequence of 10W/Al_2O_3–HY > 10W/Al_2O_3/HY > 10W/HY/Al_2O_3, which is also different from that of specific surface area, micropore volume and total acidity (10W/Al_2O_3/HY > 10W/Al_2O_3–HY > 10W/HY/Al_2O_3). It does not support a direct positive correlation between metathesis activities and these physicochemical properties. Therefore, we suggest there are other intrinsic factors to determine the metathesis activity.

As shown in Fig. 3, different preparation procedures result in the remarkable different structure of tungsten species. Upon the most active catalyst 10W/Al_2O_3–HY, Raman spectrum exhibits most intensive bands at 970 cm^{-1} and 840–880 cm^{-1}, corresponding to largest amount of isolated tetrahedral and two-dimensional surface polytungsten species. For the less active catalyst 10W/Al_2O_3/HY, we observe the same Raman bands with less intensity, indicating fewer amounts of these tungsten species. For the least active 10W/HY/Al_2O_3, it is worth noting that the 840–880 cm^{-1} band is not observed and the 970 cm^{-1} band is very weak. The sequence of intensities of bands at 970 cm^{-1} and 840–880 cm^{-1} agrees with that of metathesis activities over different catalysts. Therefore, there is a relation between the metathesis activity and structures of tungsten species. The isolated tetrahedral or two-dimensional surface polytungsten species are speculated to be the active sites precursors for the metathesis activity.

In order to obtain a further relation between metathesis activities and structure of tungsten species, the investigation is also carried out on WO_3/Al_2O_3–HY catalysts as the function of tungsten loadings. Correlating the catalytic results in Fig. 8 with the spectra in Fig. 7, a positive relation between metathesis activity and the amount of isolated tetrahedral and two-dimensional polytungsten oxide species are observed at low tungsten loading. The amount of these species and metathesis activities all increase with the increase of tungsten loading from 4 to 10 wt.%. However, this synchronous increase of tungsten species and activities can not be observed in the loading range of 10–18 wt.%. Over those catalysts, the metathesis activities still remain as high as ~62% 2-butene conversion despite the decrease of two-dimensional polytungsten species, characterized by the continuously diminished or final disappearance of 840–880 cm^{-1} Raman band. Especially for 18W/Al_2O_3–HY catalyst, without the presence of two-dimensional polytungsten species, it still achieves 61.9% 2-butene conversion. Thus, it is concluded that the diminished amount of two-dimensional surface polytungsten species does not lead to the decrease of metathesis activity. As a comparison, abundant isolated tetrahedral tungsten species, characterized by comparable intensive 970 cm^{-1} Raman bands, are all present on highly active 10W/Al_2O_3–HY, 13W/Al_2O_3-HY and 18W/Al_2O_3–HY catalysts. Consequently, the active sites should be contained in the isolated tetrahedral tungsten oxide species. This is supported by the fact that further increase of tungsten loading to 24 wt.% leads to declined 2-butene conversion of 45.5%, which is accompanied by the decrease of isolated tetrahedral tungsten species.

It should be noted that the amount of isolated tetrahedral tungsten species do not have a unilateral positive relation with the metathesis activity in the loading region of 10–18 wt.%. The 2-butene conversion is relative stable at ~62% irrespective of the variation of 970 cm^{-1} band and isolated tetrahedral tungsten oxide species. This is possibly due to the fact that the active sites are a fraction of total metal loading [32]. From Raman spectra in Fig. 7, it also can be found that WO_3 microcrystallites or highly dispersed WO_3 crystallites are present for 13W/Al_2O_3–HY and 18W/Al_2O_3–HY, which do not exhibit characteristic peaks of WO_3 crystal on XRD patterns. Although these highly dispersed crystallites species are not active for metathesis as widely reported before, they do not lead to very rapid declined activity within 3 h. However, once these microcrystallites are transformed into the bulk WO_3 crystal, as revealed by the XRD pattern of 24W/Al_2O_3–HY in Fig. 5, the quick deactivation occurs. Another possible reason for the poor initial activity and quick deactivation behavior of 24W/Al_2O_3–HY catalyst might be caused by the destroyed HY zeolite structure, as revealed by XRD and Raman spectra. It is reported that for catalysts of MoO_3 oxide catalysts supported on Hβ zeolite, the maintenance of Hβ structure is proved to be crucial for the metathesis activity [33].

5. Conclusion

Various catalysts composed of WO_3, Al_2O_3 and HY are prepared by variation of preparation procedures and tungsten loadings. XRD, UV resonance Raman and UV–vis characterization results suggest various tungsten species are co-present on different catalysts, including isolated tetrahedral tungsten species, two-dimensional surface polytungsten oxide species, WO_3-like polystructure and WO_3 crystal. The metathesis activities of these catalysts can be correlated with the structure of supported tungsten oxide species. The different preparation procedures lead to diverse tungsten species and distinctively different activities. The correlation concludes that WO_3-like polystructure and WO_3 crystal are not active in the metathesis reaction. By the study of the effect of tungsten loading, it is found that the isolated tetrahedral tungsten species are present on all active catalysts, whereas two-dimensional polytungsten species do not. As a consequence, the active sites should be contained in isolated tetrahedral tungsten oxide species, which exhibit a characteristic Raman band at 970 cm^{-1}.

Acknowledgements

The authors sincerely thank the National Natural Science Foundation of China (No. 20303019) and National 973 Project of China (No. 2003CB615802) for their financial supports.

References

[1] J.C. Mol, J. Mol. Catal. A 213 (2004) 39.
[2] R. Thomas, J.A. Moulijn, J. Mol. Catal. 15 (1982) 157.
[3] W. Grünert, R. Feldhaus, K. Anders, E.S. Shpiro, K.H.M. Minachev, J. Catal. 120 (1989) 444.
[4] A. Spamer, T.I. Dube, D.J. Moodley, C. van Schalkwyk, J.M. Botha, Appl. Catal. A 255 (2003) 153.
[5] Y. Wang, Q. Chen, W. Yang, Z. Xie, W. Xu, D. Huang, Appl. Catal. A 250 (2003) 25.
[6] A. Andreini, J.C. Mol, J. Chem. Soc., Faraday Trans. 81 (1985) 1705.
[7] R. Thomas, J.A. Moulijn, V.H.J. de Beer, J. Medema, J. Mol. Catal. 8 (1980) 161.
[8] F.P.J.M. Kerkhof, J.A. Moulijn, R. Thomas, J. Catal. 56 (1979) 279.
[9] T. Yamaguchi, Y. Tanaka, K. Tanabe, J. Catal. 65 (1980) 442.
[10] S. Huang, S. Liu, W. Xin, J. Bai, S. Xie, Q. Wang, L. Xu, J. Mol. Catal. A 226 (2005) 61.
[11] V. Logie, G. Maire, D. Michel, J.L. Vignes, J. Catal. 188 (1999) 90.
[12] J. Ramirez, A.G. Alejandre, J. Catal. 170 (1997) 108.

[13] A. De Lucas, J.L. Valverde, L. Rodriguez, P. Sanchez, M.T. Garcia, J. Mol. Catal. A 171 (2001) 195.
[14] A. de Lucas, J.L. Valverde, P. Canizares, L. Rodriguez, Appl. Catal. A 172 (1998) 165.
[15] C. Bremard, M.L. Maire, J. Phys. Chem. 97 (1993) 9695.
[16] S.S. Chan, I.E. Wachs, L.L. Murrell, N.C. Dispenziere, J. Catal. 92 (1985) 1.
[17] L. Salvati, L.E. Makovsky, J.M. Stencel, F.R. Brown, D.M. Hercules, J. Phys. Chem. 85 (1981) 3700.
[18] J.A. Horsely, I.E. Wachs, J.M. Brown, G.H. Via, F.D. Hardcastle, J. Phys. Chem. 91 (1987) 4014.
[19] M.A. Vuurman, I.E. Wachs, A.M. Hirt, J. Phys. Chem. 95 (1991) 9928.
[20] M.M. Ostromecki, L.J. Burcham, I.E. Wachs, N. Ramani, G. John, Ekerdt, J. Mol. Catal. A 132 (1998) 43.
[21] S.L. Soled, G.B. McVicker, L.L. Murrell, L.G. Gherman, N.C. Dispenziere, S.L. Hsu, D. Waldman, J. Catal. 111 (1988) 286.
[22] S. Bendezu, R. Cid, J.L.G. Fierro, A. Lopez Agudo, Appl. Catal. A 197 (2000) 47.
[23] R. Cid, J. Neira, J. Godoy, J.M. Palacios, S. Mendioroz, A. Lopez Agudo, J. Catal. 141 (1993) 206.
[24] B. Scheffer, J.J. Heijeinga, J.A. Moulijn, J. Phys. Chem. 91 (1987) 4752.
[25] A. De Lucas, J.L. Valverde, P. Canizares, L. Rodriguez, Appl. Catal. A 184 (1999) 143.
[26] L. Karakonstantis, H. Matralis, C. Kordulis, A. Lycourghiotis, J. Catal. 162 (1996) 306.
[27] D.G. Barton, S.L. Soled, G.D. Meitzner, G.A. Fuentes, E. Iglesia, J. Catal. 181 (1999) 57.
[28] S.S. Chan, I.E. Wachs, L.L. Murrell, J. Catal. 90 (1984) 150.
[29] N. Tsuda, T. Mori, N. Kosaka, Y. Sakai, J. Mol. Catal. 28 (1985) 183.
[30] D.T. Laverty, J.J. Rooney, A. Stewart, J. Catal. 45 (1976) 110.
[31] R. Spronk, J.A.R. van Veen, J.C. Mol, J. Catal. 144 (1993) 472.
[32] Y. Chauvin, D. Commereuc, J. Chem. Soc., Chem. Commun. 6 (1992) 462.
[33] S. Liu, S. Huang, W. Xin, J. Bai, S. Xie, L. Xu, Chem. Res. Chin. U 21 (2005) 213.